## Significant Findings

This paper examines spatial and temporal patterns in soil moisture and vegetation water content derived from the Land Parameter Retrieval Model throughout mainland Australia from 1998 through 2005, using TRMM/TMI passive microwave observations. Multivariate statistical techniques were used to extract dominant spatial and temporal patterns in retrieved estimates of moisture content for the top 1-cm of soil ($\theta$) and vegetation moisture content. The dominant temporal soil moisture and vegetation patterns were strongly correlated to El Niño/Southern Oscillation (ENSO) during the spring ($r^2 = 0.90$), and to a progressively lesser extent during autumn, summer, and winter. The Indian Ocean Dipole (IOD) index also explained part of the variation in springtime soil moisture and vegetation. Cluster analysis suggested that the regions most affected by ENSO are mainly located in eastern Australia. The results suggest that the drought conditions experienced in eastern Australia since 2000 and clearly indicated in the satellite retrievals, and appear to have a strong connection with ENSO patterns.

# Popular Summary

The spatial and temporal patterns in soil moisture and vegetation water content as derived by satellite throughout mainland Australia from 1998 through 2005 were investigated. Statistical techniques were used to demonstrate that temporal patterns of moisture and vegetation were strongly correlated to El Niño/Southern Oscillation (ENSO) during the spring, and to a progressively lesser extent during autumn, summer, and winter. The Indian Ocean Dipole (IOD) index also explained part of the variation in springtime soil moisture and vegetation. The analysis also suggested that the regions most affected by ENSO are mainly located in eastern Australia. The results suggest that the drought conditions experienced in eastern Australia since 2000 are clearly indicated by the satellite observations and appear to have a strong connection with ENSO patterns.

# TRMM-TMI satellite observed soil moisture and vegetation density (1998-2005) show strong connection with El Niño in eastern Australia

*Yi Liu[1,2], Richard A.M. de Jeu[1], Albert I.J.M. van Dijk[2] and Manfred Owe[3]*

[1]Vrije Universiteit Amsterdam, Faculty of Earth and Life Sciences, Dept. of Hydrology and Geo-Environmental Sciences, Amsterdam, Netherlands

[2]CSIRO Land and Water, Black Mountain Laboratory, Canberra, Australia

[3]Hydrological Sciences Branch, NASA Goddard Space Flight Center, Greenbelt, MD, USA

**Abstract**

Spatiotemporal patterns in soil moisture and vegetation water content across mainland Australia were investigated from 1998 through 2005, using TRMM/TMI passive microwave observations. The Empirical Orthogonal Function technique was used to extract dominant spatial and temporal patterns in retrieved estimates of moisture content for the top 1-cm of soil ($\theta$) and vegetation moisture content (via optical depth $\tau$). The dominant temporal $\theta$ and $\tau$ patterns were strongly correlated to El Niño/Southern Oscillation (ENSO) in spring ($r^2 = 0.90$), and to a progressively lesser extent autumn, summer and winter. The Indian Ocean Dipole (IOD) index also explained part of the variation in spring $\theta$ and $\tau$. Cluster analysis suggested that the regions most affected by ENSO are mainly located in eastern Australia. The results suggest that the drought conditions experienced in eastern Australia since 2000 and clearly expressed in these satellite observations have a strong connection with ENSO patterns.

**Keywords:** Niño/Southern Oscillation (ENSO), Indian Ocean Dipole (IOD), soil moisture, passive microwave, vegetation, ecohydrology

## 1. Introduction

Australia is subject to frequent droughts, resulting in significant impact on the economy and environment [*Horridge et al.,* 2005]. Inter-decadal phases of wetter and drier conditions are observed in rainfall records [*Beeton et al.,* 2006]. Many areas have been experiencing extraordinary drought conditions since 2000. There are questions about the possible causes of this drought: an extreme event, natural climate cycling, and/or a consequence of human-induced climate change. Rainfall patterns have been linked to several ocean circulation indicators: droughts to sea surface temperature anomalies (SSTA) over the eastern Indian Ocean [*Streten*, 1981, 1983]; winter rainfall patterns in western and southern Australia to the Indian Ocean Dipole (IOD) [*Ashok et al.*, 2003]; southeastern Queensland rainfall to central Pacific Ocean SSTA [*Murphy and Ribbe*, 2004]; and the 2001/02 drought to a modest El Niño event [*Nicholls*, 2004]. The Intergovernmental Panel on Climate Change expects rainfall to decrease in southern Australia in winter and spring and in southwestern Australia in winter, but the influence of (possibly changed) El Niño/Southern Oscillation (ENSO) patterns is uncertain [*IPCC, 2007*]. Spatial patterns, interactions, and changes in the connection between rainfall and different circulation indicators need to be better understood [*Abram et al.,* 2007] to put the current drought in appropriate context and allow statements about future drought frequency and severity to be made with greater confidence.

Soil moisture and vegetation conditions are strong indicators of antecedent weather conditions, ecosystem state and drought [*McVicar and Jupp,* 1998]. They can be inferred from satellite observations, by making use of the spectrally distinct behavior of chlorophyll in green canopies in the visible and near infrared wavebands [*Campbell,* 2002] and/or that of water in biomass and top soil in the near to thermal infrared and microwave spectra [*Choudhury,* 1993; *Fensholt and Sandholt,* 2003; *McVicar and Jupp,* 2002]. Observations of passive microwave emissions have certain advantages, in that: (i) they are available regardless of cloud cover; (ii) there is a physical relationship relating emissions to water amounts in the environment; and (iii) rather than the land surface only, they provide information on water content of the top soil layer (albeit still only a few cm deep). Potential disadvantages are the coarse resolution of observation (>10 km) and the lack of a consistent and continuous observation program over the past decades. A recently developed approach to retrieving surface parameters from microwave emissions does not require any form of field calibration and can be used for all bands in the microwave domain [*De Jeu et al.,* 2003; *Owe et al.,* 2001; *Wagner et al.,* 2007; *Owe et al.,* 2007]. This allows data collected by different satellites since 1978 to yield a time series covering 30 years.

As a first step in determining the potential use of such a longer time series, we explored the link between three ocean circulation indicators and spatiotemporal patterns in soil moisture and vegetation condition for an 8-years data set of passive microwave derived soil moisture and vegetation condition recently developed by *Owe et al.* [2007].

## 2. Data and Methods

### 2.1 Data

The Microwave Instrument (TMI) on board NASA's Tropical Rainfall Measuring Mission (TRMM) has provided operational passive microwave measurements at 10.7 GHz (X-band) and eight higher frequencies including the 37 GHz (Ka) band since December 1997 [*Kummerow et al., 1998*]. The observations can be assimilated in a microwave radiation transfer model to infer soil moisture, and a set of atmospheric, soil and vegetation variables, including soil and canopy temperature and vegetation optical depth.

We used the top soil moisture content ($\theta$ in $m^3$ $m^{-3}$) retrieved using the Land Parameter Retrieval Model (LPRM) [*Owe et al.,* 2001; *De Jeu et al.*, 2003; *Meesters et al.*, 2005] and X-band brightness temperature. The retrieved soil moisture is represents roughly the top 1-cm, because TMI with the low observing frequency of 10.7 GHz (X-band) has a source depth of about 1 cm. It has been evaluated against various observational and simulated datasets, generally with good results and with an absolute accuracy of ca. 0.06 $m^3$ $m^{-3}$ [*Owe et al.,* 2001, *De Jeu and Owe,* 2003, *O' Neill et al.,* 2006, *Wagner et al.,* 2007].

Vegetation optical depth ($\tau$) is a dimensionless parameter that can be interpreted as being directly proportional to vegetation water content [*Jackson and O'Neill,* 1990;

*Jackson and Schmugge,* 1991] and was derived according to *Meesters et al.* [2005]. The retrieved soil moisture and vegetation optical depth data were resampled and aggregated into seasonal average 0.25° resolution images for December 1997 through December 2005 for mainland Australia. Two spring seasons - one wet, the other dry - are shown in Figure 1. Areas where observations are influenced by open water or snow are left white.

[FIGURE 1 ABOUT HERE]

The ocean circulation indicators used in this study were the ENSO index, the North Atlantic Oscillation (NAO) and the Indian Ocean Dipole (IOD) Mode Index. The ENSO index is obtained from Bureau of Meteorology of Australia (http://www.bom.gov.au/climate/current/soihtm1.shtml), IOD index from *Saji et al.* [1999] (http://www.jamstec.go.jp/frsgc/research/d1/iod/) and NAO index from National Oceanic and Atmospheric Administration (NOAA, ftp://ftp.cpc.ncep.noaa.gov/wd52dg/data/indices/tele_index.nh). The ENSO index is the sea surface temperature anomaly from the 5°S to 5°N and 90°W to 150°W in the equatorial tropical Pacific [*Reynolds and Smith*, 1994]. *Saji et al.* [1999] defined the IOD index as the sea surface temperature difference between the tropical western Indian Ocean (10°S-10°N, 50°E-70°E) and the tropical southeastern Indian Ocean (10°S-equator, 90°E-110°E). The NAO index is constructed by comparing daily 500 mb height anomalies over the Northern Hemisphere to monthly mean 500 mb air pressure height for 1950 through 2000 [*Barnston and Livezey, 1987*].

## 2.2 Methods

Empirical Orthogonal Function (EOF) analysis, Spearman's rank correlation analysis and K-means cluster analysis were used in this analysis. EOF analysis [*Bjornsson et al.*, 2000] produces a set of functions that represent various modes of oscillation dominating in a spatiotemporal data set, and the relative importance of each pattern in explaining observed variation across space. EOF analysis has been applied to study correlation between Northern Hemisphere air temperature and satellite-derived greenness, and ENSO and Arctic Oscillation [*Buermann et al.,* 2003]. Here the EOF analysis was performed on seasonal averages of $\theta$ and $\tau$, and Spearman's rank correlation coefficients were calculated between the first two EOFs of each observation and the ENSO, IOD and NAO indicators.

We applied K-means cluster analysis [*Dillon and Goldstein,* 1984] to the first EOFs of $\theta$ and $\tau$ to identify regions of Australia with different sensitivity to ocean circulation indicators. The technique groups objects, or data, into a smaller number K of clusters with data that are as close to each other and as far from other clusters as possible. K-means cluster analysis has been widely applied in soil and vegetation research, *e.g.* for remotely sensed land cover classification [*Han et al.*, 2004], regionalizing watersheds in flood-frequency analysis [*Rao et al.* 2006], and weather classification for rainfall simulation [*Wilson et al.,* 1991].

## 3. Results

The variances explained by the first four EOFs for $\theta$ and $\tau$ of four seasons are listed in

Table 1. Ranked correlation coefficients between the leading two EOFs and ENSO, IOD and NAO indices are listed in Table 2. The respective EOFs for θ and τ are reasonably well correlated for most of the year, but in winter both τ-EOFs appear correlated to θ-EOF2 but not to θ-EOF1, and in summer the respective second EOFs are not correlated at all. In other words, the coupling between θ and τ appears strongest in spring and autumn, and least in winter.

[TABLES 1 AND 2 ABOUT HERE]

The θ-EOF1 for all seasons and τ-EOF1 for spring and autumn are moderately to strongly correlated to ENSO. The strongest correlations ($r^2$=0.90) are for spring (Table 2) and these correlations are in phase (Figure 2). Wet seasons correspond to higher than average ENSO (1998-2001) and dry seasons to lower than average ENSO (2002-2005).

[FIGURE 2 ABOUT HERE]

In addition, θ-EOF1 is significantly correlated to IOD in spring. The coefficient of correlation is greater than that between ENSO and IOD, which suggests that this is not merely a spurious correlation. While not significant at 0.05 level, the correlation between θ-EOF1 and NAO in winter is still high ($r^2$=0.48).

The spatial structures of the first EOFs for spring θ and τ show that these signals are strongest in eastern Australia, in particular in eastern Queensland and the eastern Murray-Darling Basin (Figure 3).

[FIGURES 3 ABOUT HERE]

K-means cluster analysis was performed using the first EOFs for spring θ and τ and for two to ten clusters. The results suggested only two significant clusters (Figure 4; silhouette value 0.74). Region 1 (dark gray) represents the areas with the highest correlations between spring θ and τ and ENSO, respectively.

[FIGURE 4 ABOUT HERE]

## 4. Discussion and Conclusions

For the period 1998 through 2005, we found a strong correlation between seasonal soil and vegetation moisture content derived from passive microwave observations and ENSO, particularly for eastern Australia in spring, and also for autumn and summer. In addition, we found a signal relating both θ and τ to IOD in spring.

The influence of ENSO on rainfall has been documented [e.g. *McBride and Nicholls*. 1983; *Whetton*, 1997], as has that of IOD [*Simmonds*, 1990; *Drosdowsky*, 2002; *Saji et al.*, 1999]. Apart from confirming these findings, our results provide evidence that ENSO, and to a lesser extent IOD, can also be linked to the drought conditions experienced since 2000. It shows that the ENSO/IOD influence on rainfall is also evident in the soil moisture and vegetation record.

Without using station rainfall records, we were able to directly delineate regions experiencing the strongest influence of ENSO. The most affected regions are in the eastern Murray-Darling Basin and eastern Queensland on the inland side of the Great Dividing Range; both are important agricultural regions.

Development of a longer time series of global data of soil moisture, vegetation optical depth and surface temperature composited from different passive microwave observation sources should allow us to better understand seasonal and inter-annual variations in climate associated with ocean circulation patterns.

## References


Abram, N. J., M. K. Gagan, Z. Liu, W. S. Hantoro, M. T. McCulloch, and B. W. Suwargadi (2007), Seasonal characteristics of the Indian Ocean Dipole during the Holocene epoch, *Nature, 445,* 299-302, doi:10.1038/nature05477.

Ashok, K., Z. Guan, and T. Yamagata (2003), Influence of the Indian Ocean Dipole on the Australian winter rainfall, *Geophys. Res. Lett., 30*(15), 1821, doi: 10.1029/2003GL017926.

Barnston A.G., and R.E. Livezy, (1987), Classification, Seasonality and Persistance of Low-Frequency Atmospheric Circulation Patterns. *Mon. Wea. Rev., 115,* 1083-1126.

Beeton, R.J.S., K.I. Buckley, G.J. Jones, D. Morgan, R.E. Reichelt, and T. Dennis (2006) , *Australia State of the Environment 2006*, Independent report to the Australian Government Minister for the Environment and Heritage, Department of the Environment and Heritage, Canberra.

Bjornsson, H., and S. A. Venegas (2000), *A manual for EOF and SVD analyses of Climatic Data,* 53 pp, McGill University., Montreal, Canada.

Buermann, W., B. Anderson, C.J. Tucker, R.E. Dickinson, W. Lucht, C.S. Potter, and R.B. Myneni (2003), Interannual covariability in Northern Hemisphere air temperatures and greenness associated with El Niño-Southern Oscillation and the Arctic Oscillation. *J. Geophys. Res., 108*(D13), 4396, doi: 10.1029/2002JD002630.

Campbell, J. B. (2002), *Introduction to remote sensing (3rd Edition)*, The Guilford Press, New York.

Choudhury, B.J. (1993), Desertification, In: Atlas of Satellite Observations related to Global Change, (Eds, R.J. Gurney, J.L. Foster, C.L. Parkinson) , Cambridge University Press New York, 313-326

De Jeu, R.A.M. and M. Owe (2003), Further Validation of a New Methodology for Surface Moisture and Vegetation Optical Depth Retrieval, *Int. J. Remote Sens., 24,* 4559-4578.

Dillon, W.R., and M. Goldstein (1984), *Multivariate Analysis: Methods and Applications,* John Wiley & Sons, New York.

Drosdowsky, W. (2002), SST phases and Australian rainfall. *Aust. Meteorol. Mag.,51,* 1-12.

Fensholt, R., and I. Sandholt (2003), Derivation of a shortwave infrared water stress index from MODIS near- and shortwave infrared data in a semiarid environment. *Rem. Sens. Environ., 87,* 111-121.

Han, K.S., J.L. Champeaux, and J.L. Roujean (2004), A land cover classification product over France at 1 km resolution using SPOT4/VEGETATION data. *Rem. Sens. Environ., 92*, 52–66, doi:10.1016/j.rse.2004.05.005.

Horridge, M., J. Madden, and G. Wittwer (2005), The impact of the 2002-2003 drought on Australia, *J. Pol. Modeling,* 85-308,doi:10.1016/j.jpolmod.2005.01.008.

IPCC (2007), Climate Change 2007: The Physical Science Basis, Summary for Policymakers. http://www.ipcc.ch/press/SPM.pdf

Jackson, T.J. and P.E. O'Neill (1990), Attenuation of soil microwave emission by corn and soybeans at 1.4 and 5 GHz. *IEEE Trans. Geosci. Remote Sensing, 28*,978-980.

Jackson, T.J. and T.J. Schmugge (1991), Vegetation effects on the microwave emission from soils, *Rem. Sens. Environ., 36,*203-212.

Kummerow, C., W. Barnes, T. Kozu, J. Shiue, and J. Simpson, (1998), The Tropical Rainfall Measuring Mission (TRMM) sensor package, *J. Atm. Oceanic Tech., 15,* 809-817.

McBride, J.L., N. Nicholls (1983), Seasonal relationships between Australian rainfall and the southern oscillation. *Mon. Wea. Rev., 111,* 1998-2004.

McVicar, T.R. and D.L.B. Jupp (1998), The current and potential operational uses of remote sensing to aid decisions on drought exceptional circumstances in Australia: a review. *Agr. Syst., 79*(2), 399-468.

McVicar, T.R. and D.L.B. Jupp (2002), Using covariates to spatially interpolate moisture availability in the Murray-Darling Basin: a novel use of remotely sensed data. *Rem. Sens. Environ., 79*, 199-212.

Meesters, A.G.C.A., R.A.M. de Jeu, and M. Owe (2005), Analytical derivation of the vegetation optical depth from the microwave polarization difference index, *IEEE Trans. Geosci. Remote Sensing, 2*(2):121-123.

Murphy, F., and J. Ribbe (2004), Variability of southeastern Queensland rainfall and climate indices, *Int. J. Climatol., 24,* 703–721.

Nicholls, N, (2004), The changing nature of Australian droughts. *Climatic Change, 63,* 323-336.

O'Neill, P.E., E.G. Njoku, J. Shi, E.F. Wood, M. Owe, and B. Gouweleeuw (2006), Hydros Soil Moisture Retrieval Algorithms: Status and Relevance to Future Missions, Proc. IGARSS 2006.

Owe, M., R.A.M. De Jeu, and J.P. Walker (2001), A Methodology for Surface Soil Moisture and Vegetation Optical Depth Retrieval Using the Microwave Polarization Difference Index, *IEEE Trans. Geosci. Remote Sensing, 39*(8), 1643-1654. doi: 10.1109/36.942542.

Owe, M., R.A.M. De Jeu and T. Holmes (2007), Multi-Sensor Historical Climatology of Satellite-Derived Global Land Surface Moisture, *J. Geophys. Res.,* submitted.

Reynolds, R.W., and T.M. Smith (1994) Improved global sea surface temperature analysis using optimum interpolation, *J. Clim., 7,* 929-948

Rao, A.R., and V.V.Srinivas (2006), Regionalization of watersheds by hybrid-cluster analysis. *J. Hydrol., 318*, 37-56, doi:10.1016/j.jhydrol.2005.06.003.

Saji, N.H., B.N. Goswami, P.N. Vinayachandran, and T, Yamagata (1999), A dipole mode in the tropical Indian Ocean. *Nature, 401*, 360–363.

Simmonds, I. (1990), A modeling study of winter circulation and precipitation anomalies associated with Australian region ocean temperatures. *Aust Meteorol Mag., 38,* 151-161.

Streten, N. A. (1981), Southern hemisphere sea surface temperature variability and apparent associations with Australian rainfall. *J. Geophys. Res., 86*, 485–497.

Streten, N. A. (1983), Extreme distributions of Australian rainfall in relation to sea surface temperature. *J. Climatol., 3*, 143–153.

Wagner, W., V. Naeimi, K. Scipal, R. De Jeu, and J. M. Fernandez (2007), Soil Moisture from Operational Meteorological Satellites, *Hydrogeol. J., 15,* 121-131, doi: 10.1007/s10040-006-0104-6

Whetton, P.H. (1997), Floods, droughts and the Southern Oscillation connection. In: Windows on Meteorology: Australian Perspective (ed. Webb, E.K.), 180-199pp, CSIRO Publishing, Melbourne.

Wilson, L.L., D.P. Lettenmaier, and E.F. Wood (1991), Simulation of daily precipitation in the Pacific Northwest using a weather classification scheme. *Surv. Geophys., 12*, 127-142.

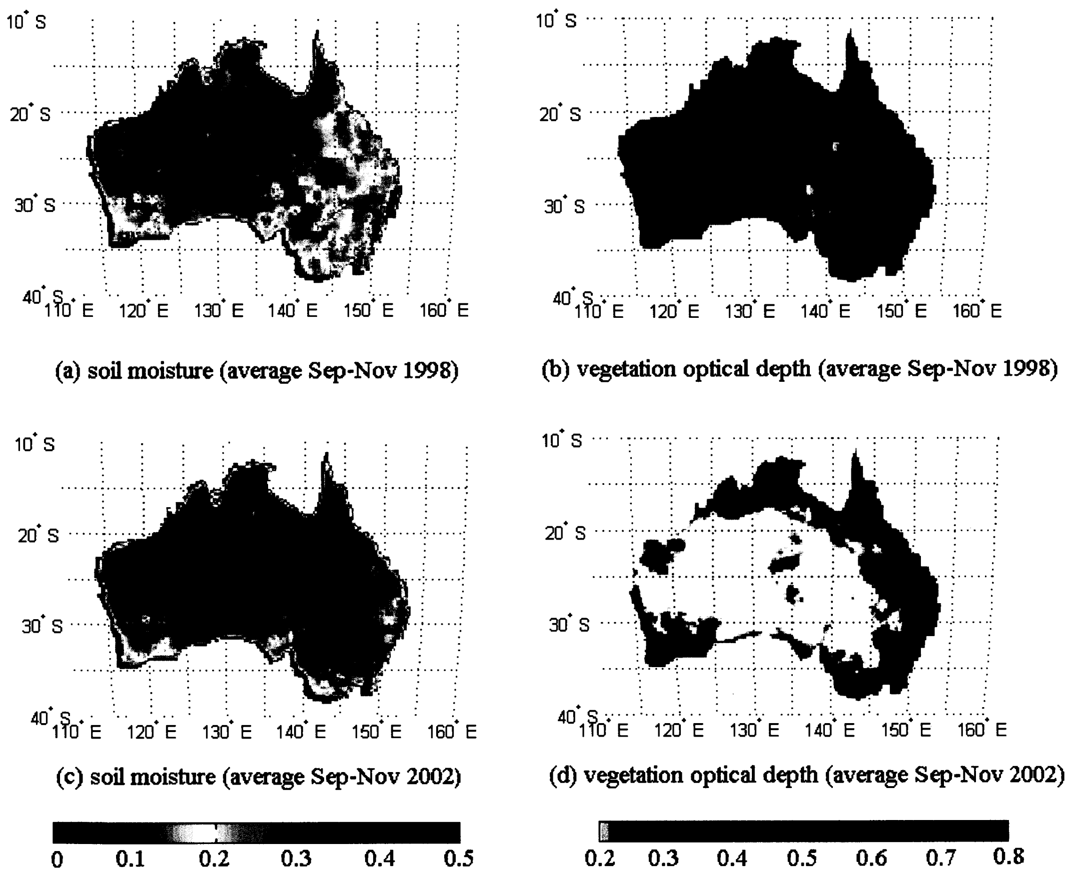


**Figure 1.** Average soil moisture (θ in $m^3$ $m^{-3}$) in top 1-cm of soil and vegetation optical depth (τ) for a wet spring (September-November 1998) and a dry spring (2002) across mainland Australia.

**Table 1.** Variance explained (%) by the first four EOF patterns in soil moisture (θ) and vegetation optical depth (τ) for four seasons.

| | EOF1 (%) | EOF2 (%) | EOF3 (%) | EOF4 (%) | Total (%) |
|---|---|---|---|---|---|
| Spring θ | 57 | 13 | 10 | 6 | 86 |
| Spring τ | 56 | 17 | 11 | 6 | 90 |
| Summer θ | 41 | 17 | 15 | 8 | 81 |
| Summer τ | 59 | 13 | 11 | 5 | 88 |
| Autumn θ | 59 | 16 | 7 | 6 | 88 |
| Autumn τ | 62 | 13 | 8 | 5 | 88 |
| Winter θ | 38 | 21 | 12 | 11 | 82 |
| Winter τ | 61 | 16 | 6 | 5 | 88 |

**Table 2.** Spearman correlation coefficients ($r^2$) between the leading two EOF patterns of soil moisture (θ) and vegetation optical depth (τ) of the four seasons, and ENSO, IOD and NAO indices. Tables are diagonally split: all values for one season are in the bottom-left half; all values for another season in the top-right half. Suffixes [a] and [b] represent indicate correlations significant at 0.01 and 0.05 level, respectively.

| Summer / Spring | θ EOF1 | θ EOF2 | τ EOF1 | τ EOF2 | ENSO | IOD | NAO |
|---|---|---|---|---|---|---|---|
| θ EOF1 | | 0.00 | 0.54[b] | 0.00 | 0.69[b] | 0.07 | 0.08 |
| θ EOF2 | 0.01 | | 0.02 | 0.00 | 0.05 | 0.23 | 0.16 |
| τ EOF1 | 0.90[a] | 0.01 | | 0.00 | 0.48 | 0.38 | 0.07 |
| τ EOF2 | 0.10 | 0.25 | 0.02 | | 0.06 | 0.07 | 0.38 |
| ENSO | 0.90[a] | 0.00 | 0.90[a] | 0.08 | | 0.00 | 0.25 |
| IOD | 0.58[b] | 0.02 | 0.41 | 0.20 | 0.48 | | 0.10 |
| NAO | 0.04 | 0.05 | 0.13 | 0.01 | 0.06 | 0.01 | |

| Autumn \ Winter | θ EOF1 | θ EOF2 | τ EOF1 | τ EOF2 | ENSO | IOD | NAO |
|---|---|---|---|---|---|---|---|
| θ EOF1 | | 0.10 | 0.13 | 0.18 | 0.77[b] | 0.05 | 0.48 |
| θ EOF2 | 0.01 | | 0.51[b] | 0.51[b] | 0.23 | 0.01 | 0.03 |
| τ EOF1 | 0.73[b] | 0.00 | | 0.04 | 0.06 | 0.01 | 0.25 |
| τ EOF2 | 0.02 | 0.77[b] | 0.02 | | 0.58[b] | 0.01 | 0.07 |
| ENSO | 0.69[b] | 0.00 | 0.66[b] | 0.03 | | 0.04 | 0.13 |
| IOD | 0.41 | 0.00 | 0.15 | 0.16 | 0.50 | | 0.20 |
| NAO | 0.13 | 0.00 | 0.18 | 0.02 | 0.23 | 0.05 | |

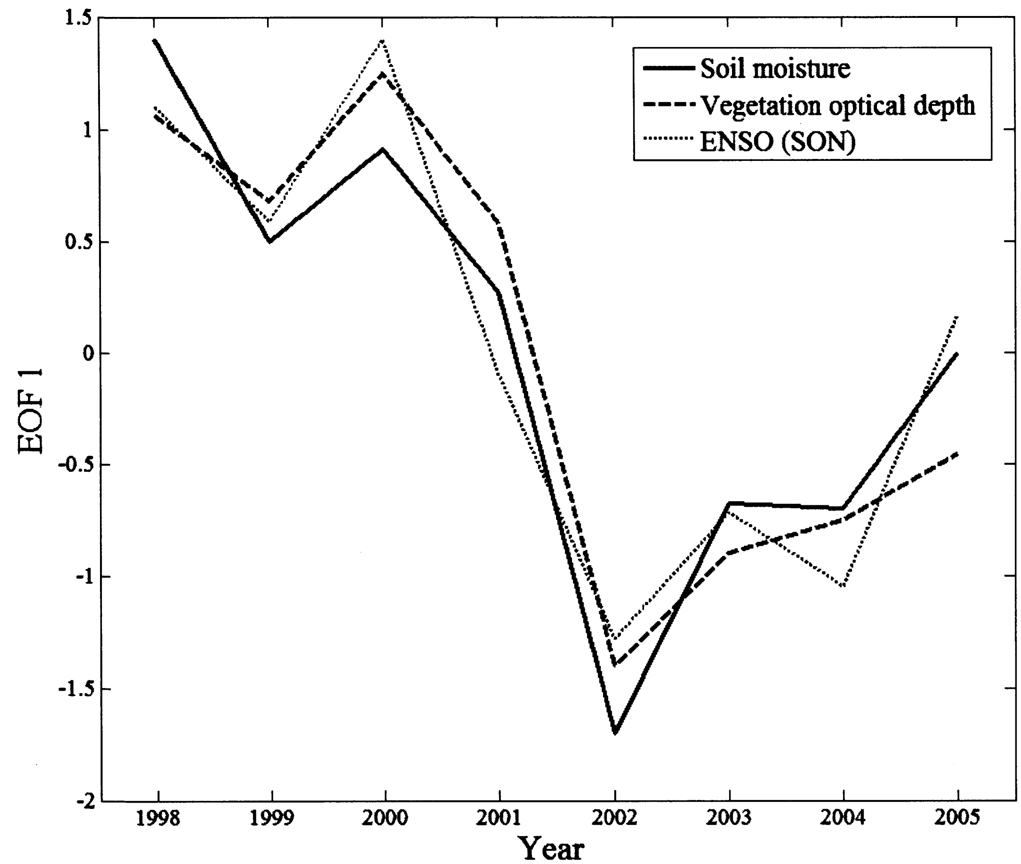


**Figure 2.** Normalized time series of the first EOFs of spring (September-November) $\theta$ and $\tau$ and the ENSO index for the period 1998-2005. Data shown as anomalies from the mean normalized by standard deviation.

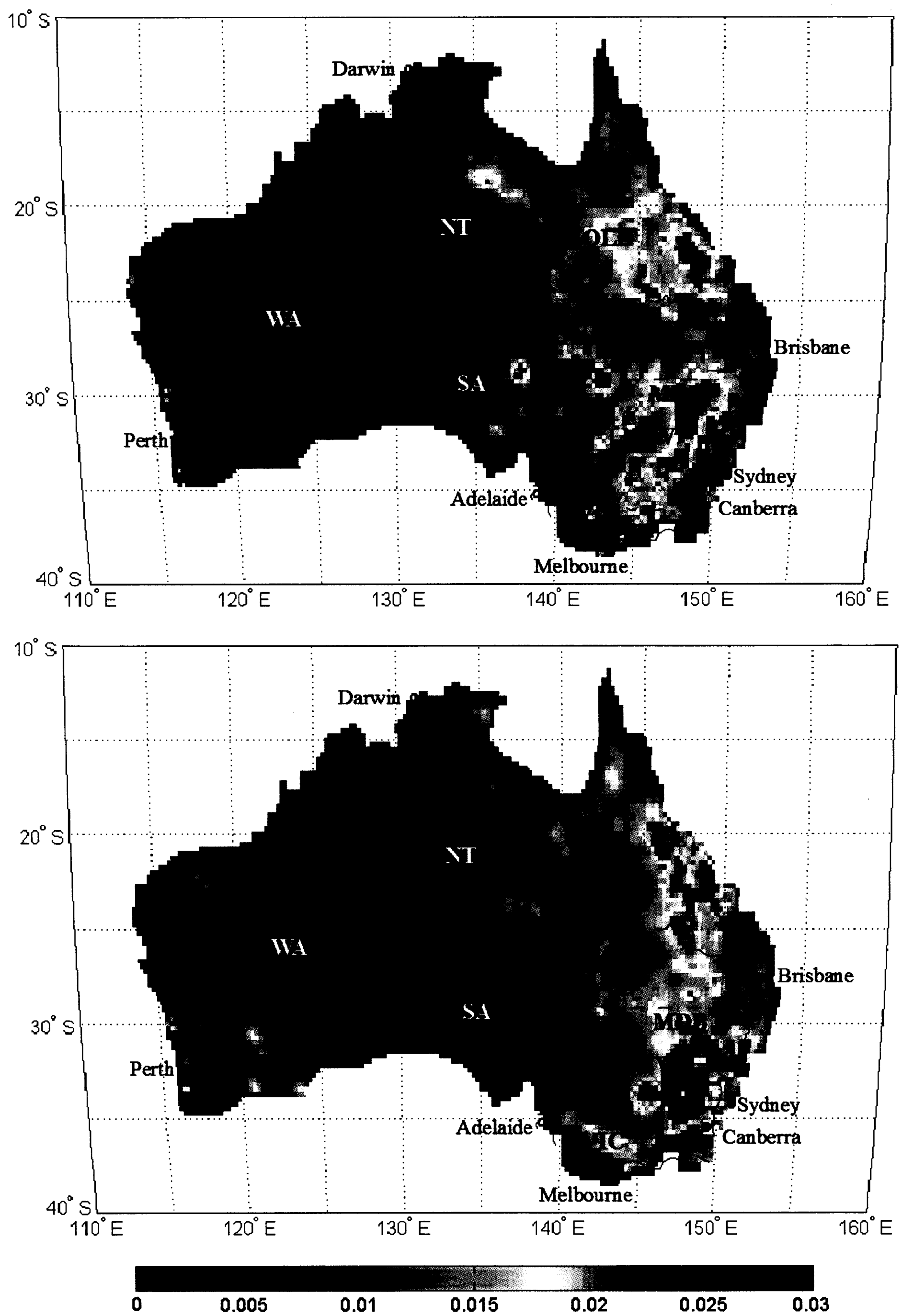


**Figure 3.** The first EOF pattern in spring (September to November) for **(a)** soil moisture (θ), explaining 57% of total variation; and **(b)** vegetation optical depth (τ), explaining 56% of total variation. WA—Western Australia, NT—Northern Territory, QLD—Queensland, SA—South Australia, NSW—New South Wales, VIC—Victoria,

MDB—Murray Darling Basin.

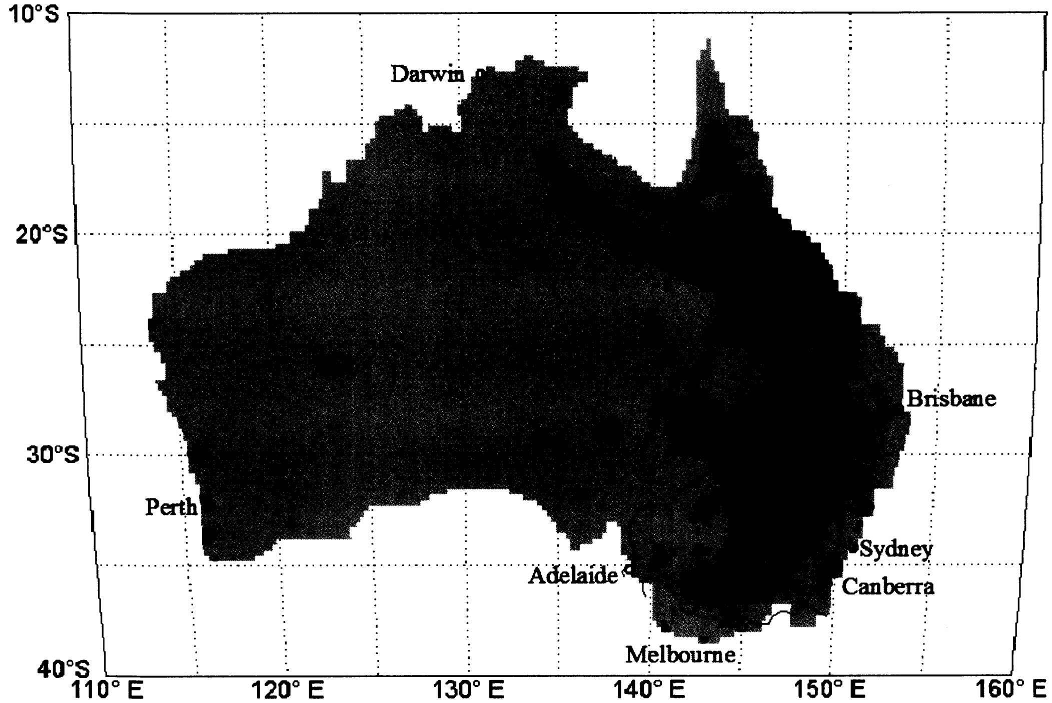


**Figure 4.** Location of the two classes derived from K-means clustering analysis based on Figure 3. In black the cluster for which both soil moisture and vegetation are relatively strongly correlated to ENSO (the centers are 0.016 for $\theta$ and 0.015 for $\tau$); in grey areas less strong correlations (the centers are 0.004 for $\theta$ and 0.006 for $\tau$).